Modeling, Identification and Control, Vol. 39, No. 1, 2018, pp. 23–35, ISSN 1890–1328

Flow Characteristics and Sizing of Annular Seat Valves for Digital Displacement Machines

C. Noergaard [1] M. M. Bech [1] T. O. Andersen [1] J. H. Christensen [1]

[1] *Fluid Power and Mechatronic Systems Section, Department of Energy Technology, Aalborg University, 9220 Aalborg, Denmark. E-mail:* {chn, mmb, toa, jhc}@et.aau.dk

Abstract

This paper investigates the steady-state flow characteristics and power losses of annular seat valves for digital displacement machines. Annular seat valves are promising candidates for active check-valves used in digital displacement fluid power machinery which excels in efficiency in a broad operating range. To achieve high machine efficiency, the valve flow losses and the required electrical power needed for valve switching should be low. The annular valve plunger geometry, of a valve prototype developed for digital displacement machines, is parametrized by three parameters: stroke length, seat radius and seat width. The steady-state flow characteristics are analyzed using static axi-symmetric computational fluid dynamics. The pressure drops and flow forces are mapped in the valve design space for several different flow rates. The simulated results are compared against measurements using a valve prototype. Using the simulated maps to estimate the flow power losses and a simple generic model to estimate the electric power losses, both during digital displacement operation, optimal designs of annular seat valves, with respect to valve power losses, are derived under several different operating conditions.

Keywords: digital fluid power, CFD analysis, active check-valves, annular seat valve.

1 Introduction

Digital Displacement Machines (DDMs), often also referred to as digital pumps/motors, are promising candidates for improving the achievable efficiency of fluid power machinery (pumps and motors). DDMs use several parallel configured cylinders, each connected to high- and low-pressure manifolds through two electrically controlled fast switching on/off valves. By controlling the valves appropriately with respect to the reciprocating piston of the cylinder, motoring-, pumping- and idling-operation cycles are obtained (Rampen, 2010). When idling, the cylinder is effectively disabled by keeping the low-pressure valve open throughout the operation cycle, resulting in low losses from "breathing" oil back and forth from the low-pressure manifold. The total machine displacement may be controlled, by the number of active versus idling cylinders. This enables maintaining efficient operation in a broad operating range, since the machine losses scale close to linearly with the displacement opposed to typical fluid-power machinery as can be observed from Figure 1.

For efficient high-speed operation of DDMs the active check-valves must:

- be fast switching, in order to minimize the amount of flow conducted with semi-opened valves (Roemer et al., 2013),
- impose a low pressure drop to maintain high efficiencies at low displacement ratios (Merrill et al., 2010),
- Consume electrical power below 1-2% of the average power of active strokes (Linjama and Huhtala, 2009) .

In addition to the performance requirements listed above, the valves must endure billions of cycles during

doi:10.4173/mic.2018.1.3

NOMENCLATURE

θ	Shaft angle [rad]
Q	Flow rate [L/min]
p	Pressure [bar]
z	Plunger position [m]
L_{stroke}	Valve lift [m]
R_{seat}	Mean radius of plunger seat [m]
W_{seat}	Seat width [m]
N_{holes}	No. of port bore holes [-]
Re, Re_{c}	Reynolds No., Critical Reynolds No. [-]
C_{d}	Discharge coefficient [-]
k_{f}	Flow-pressure coefficient $[\sqrt{pa} \cdot s/m^3]$
D_{h}	Hydraulic $\oslash$ [m]
L_{c}	Characteristic length [m]
P_{w}	Wetted perimeter [m]
T_{s}	Valve switching time [s]
ρ_{oil}, ν_{oil}	Density, Kin. viscosity [kg/m^3, m^2/s]
E, P	Energy, Power [J, W]
ϵ_{loss}	Loss fraction [%]
η	Efficiency [%]

ACRONYMS

AIP	Artemis Intelligent Power Ltd.
DDM	Digital Displacement Machine
LPV, HPV	Low- and High-pressure valve
CFD	Computational Fluid Dynamics
PT	Prototype

their lifespan for several of the proposed application targets e.g. wind turbines and wave energy harvesting machinery (Roemer, 2014). To meet these demands, the technology pioneers Artemis Intelligent Power Ltd. (AIP) uses direct electro-magnetically actuated annular seat check-valves whereas other explored approaches rely on two-stage bi-directional check-valves (Holland et al., 2011) or direct electro-magnetically actuated on/off valves without check-valve capability (Heikkila et al., 2010). When using valves with check-valve capability a passive force element, such as a spring or a permanent magnet, is used to return to the valve to the normal state. AIP uses normally opened valves for the LPV and normally closed valves for the HPV (Roemer, 2014). Normally opened valves only require electrical power during the closing (valve is kept closed by pressure forces) opposed to normally closed valves which requires electrical power both to open and to remain open during flow conduction. This paper focuses on normally opened valves where the magnitude of the axial flow forces acting to close the valve during the peak flow rate sets the requirements to the strength of the passive opening element since it must keep the valve open. Therefore, the electrical power needed for closing the valve is strongly influenced by the magnitude of the passive opening force since the actuator is working against it.

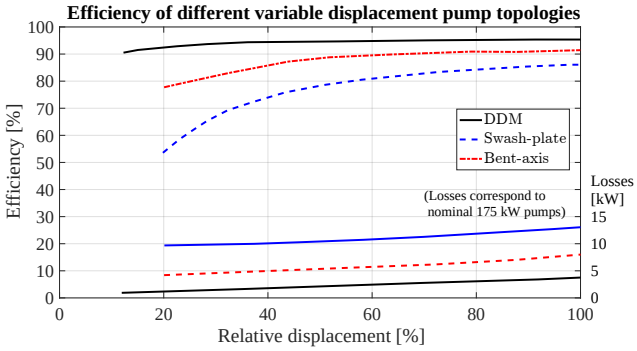

Figure 1: Comparison of measured efficiency of an automotive scale 175 kW DDM against the more developed Bent-axis and Swash-plate variable displacement type pump topologies, based on graphs published in Taylor et al. (2011). The revolution speed is 1500 RPM.

DDMs have been proposed for several purposes e.g. hydro-static transmission systems, direct cylinder motion control (Heikkila, 2016) and energy-storage systems in hybrid vehicles (Taylor et al., 2015). For low-speed applications of DDMs, such as hydraulic winches (Nordaas et al., 2017), the valves do not require to be as fast and commercial valves meeting the requirements do exist. However, understanding the valve power losses is still important to ensure high machine efficiency.

Initially, the performance requirements to the valves of DDMs are discussed in terms of valve pressure drop and valve switching time for enabling efficient DDM operation. Then, an analysis of the flow field in annular seat valves is presented based on both numerical methods and laboratory measurements. Finally, based on a large number of model evaluations, optimal valve designs are identified for a wide range of valve flow rates and switching times (corresponding to machine revolution speeds) using a simple generic model for estimation of the valve power losses during DDM operation. The results allow identification of optimal designs and the dominating valve power losses, for a wide range of annular seat valve geometries and under different operating conditions.

2 Background

In Roemer et al. (2013) general valve requirements for DDMs in terms of switching time and pressure drop are set forth based on a simple generic dynamic model of a single pressure chamber incl. the two associated on/off valves. The part-load efficiency at 20% displacement and 350 bar machine pressure span was mapped, us-

ing normalized switching-time and flow-pressure coefficients, concluding that the valve switching time should be below 5% of the revolution time since the efficiency drops severely at larger switching times. For high-efficient part-load operation (95-99%) the normalized flow-pressure coefficient[1] should be in the range 2-5%. Using the Orifice Equation, this corresponds to valve pressure drops at the peak flow rate of 0.52-2.16 bar or 0.15-0.72% of the machine pressure span. If assuming a discharge coefficient of 0.6 and a oil density of 770 kg/m^3, this corresponds to discharge areas of 4.95-1.02 cm^2 respectively.

In Merrill et al. (2010) an efficiency comparison of DDMs against valve plate design based fluid power pumps and motor. The authors conclude that DDMs are *"an extremely promising technology in being able to make a breakthrough in improving the overall efficiency especially at low displacements of variable displacement pump/motors"*. The analysis is based on simulation of a 7 piston 30 CC pump running at 3000 RPM and 300 bar machine pressure span. This corresponds to peak valve flows 40.4 L/min where valves with discharge areas of 0.4 cm^2 are found suitable. Using the Orifice Equation with the same assumptions as above, this corresponds to a valve pressure drop at the peak flow rate of 1% of the machine pressure span.

In Roemer et al. (2016) the valve sizing for a DDM was investigated through optimization based on lumped models similar to, but slightly more advanced than the lumped models the analysis of Roemer et al. (2013) was based upon. A single DDM chamber model was used to evaluate the efficiency when using different valve design parameters. The optimization results identify optimal valve parameters i.e. mean seat radius and valve stroke length. A DDM chamber of 190 CC running at 1000 RPM (corresponding to a maximum flow rate of approx. 600 L/min) has optimum efficiency with a stroke length for the HPV and LPV of 3-5 mm and 5-7 mm, respectively. The stroke length of the LPV should be larger to maintain high efficiencies when operating at low displacement ratios. The required actuator force for switching the valves sufficiently fast is approximately 600-800 N. An optimum design point was studied further, having a mean seat radius of approximately 30 mm for both valves. The valve switching required approximately an average of 50-70 W mechanical work resulting in efficiency, at only 10% machine displacement, of impressive 92.7%. The efficiency calculation includes the flow losses (incl. estimate of the manifold flow losses), compression losses and the mechanical switching losses but not mechanical friction losses or the losses originating from conversion of electric power to mechanical work through direct electro-magnetic actuators. The electric power losses are important to understand and should at maximum only constitute a few percent of the machine power to retain high efficiencies (Linjama and Huhtala, 2009). In Noergaard et al. (2016) an optimization of a moving coil actuated check-valve applied in a DDM was carried out which showed the electrical losses and the flow losses, to be of comparable magnitude, at full machine displacement for 50 CC chamber's running at 800 RPM.

In Tammisto et al. (2010), a DDM pump was experimentally tested which utilizes commercial, but slightly modified MOOG NS6 4-way directional spool valves ($T_s \approx 5{-}7$ ms and $\Delta p_{\text{valve}} = 5$ bar @ 70 L/min). The pump uses three parallel connected pistons, each with a displacement volume of 9 CC per revolution. Running the pump at 1000 RPM with machine pressure span of 120 bar resulted in efficiencies of approximately 80% at full displacement. However at 20% displacement, the efficiency drops to approximately 66%. The poor efficiency is subscripted to electrical inefficient solenoid actuators, valve leakage and excessive valve pressure losses.

3 Flow Field of Annular Seat Valves

An analysis of the valve flows throughout the geometry design space is carried out to understand the nature of the flow and to aid in selecting the best suited flow model for CFD analysis. Initially, Reynolds numbers are calculated analytically for three different flow restrictions in the fluid-flow path indicated in Figure 2.

Initially, attention is turned to the seat restriction. The Reynolds number is defined as:

$$\text{Re} = \frac{uL_c}{\nu_{\text{oil}}}, \tag{1}$$

where u is the flow velocity, L_c is a characteristic linear dimension and ν_{oil} is the kinematic oil viscosity. Assuming a uniform flow distribution in the seat restriction region, the Reynolds number may be rewritten as:

$$\text{Re} = \frac{QD_h}{A_{\text{flow}}\nu_{\text{oil}}}, \tag{2}$$

with the hydraulic diameter being $D_h = 4A_{\text{flow}}/P_w$, where P_w is the wetted perimeter. In the case of annular seat valves, the hydraulic diameter is equal to $2L_{\text{stroke}}$ (Merritt, 1967) and hence (2) for the seat restriction reduces to

$$\text{Re}_{\text{seat}} = \frac{Q}{2\pi R_{\text{seat}}\nu_{\text{oil}}}, \tag{3}$$

[1] Normalized flow-pressure coefficient $\overline{k}_f = \frac{k_f}{\frac{\sqrt{\Delta p_{\text{machine}}}}{Q_{\text{avg}}}}$ used in the orifice model $Q = \frac{1}{k_f}\sqrt{\Delta p_{\text{valve}}}$.

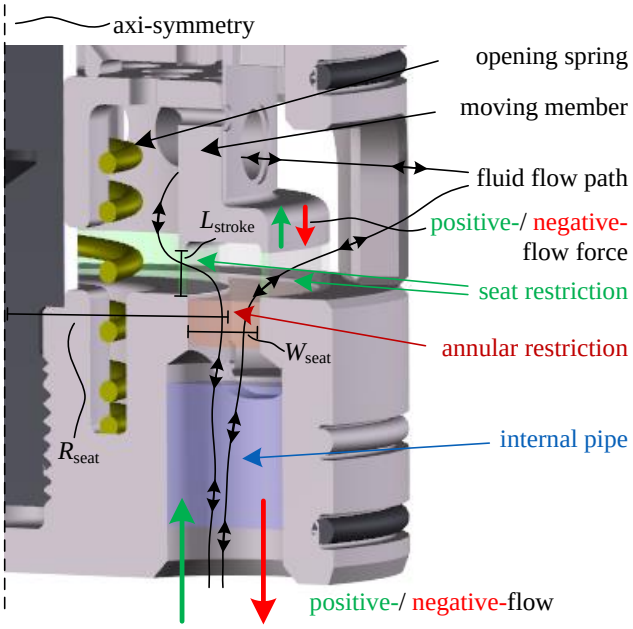

Figure 2: Illustration of the restrictions the Reynolds number is calculated for. The valve design is a moving coil actuated seat valve PT for DDMs, derived in Noergaard et al. (2016). Also, direction of flow and flow forces are defined.

showing that the Reynolds number is independent of the valve stroke length (or plunger position) since the velocity and characteristic length product of (1) remains constant with changes in stroke length. Next, attention is turned towards the annular restriction underneath the valve plunger. The hydraulic diameter is $2W_{\text{seat}}$ making the Reynolds number

$$\text{Re}_{\text{annulus}} = \frac{Q}{\pi R_{\text{seat}} \nu_{\text{oil}}}. \tag{4}$$

Again, the only geometric variable governing the Reynolds number is the seat radius. Finally, the Reynolds number for the bottom valve bores are treated as internal pipe flow assuming a flow rate of Q/N_{holes} through each bore:

$$\text{Re}_{\text{pipe}} = \frac{2Q}{\pi R_{\text{bore}} N_{\text{holes}} \nu_{\text{oil}}}, \tag{5}$$

where R_{bore} is the radius of outlet bore and N_{holes} is the number of outlet bore holes. Evaluating (3) through (5) as a function of the seat radius gives the results shown in Figure 3. Three flow rates of 100, 250 and 700 L/min are used, the number of outlet holes is set to eight and the outlet bore radius is $R_{\text{bore}} = \frac{R_{\text{seat}}}{4}$ based on the valve PT of Figure 2. All Reynolds numbers decrease inversely proportional with the seat radius.

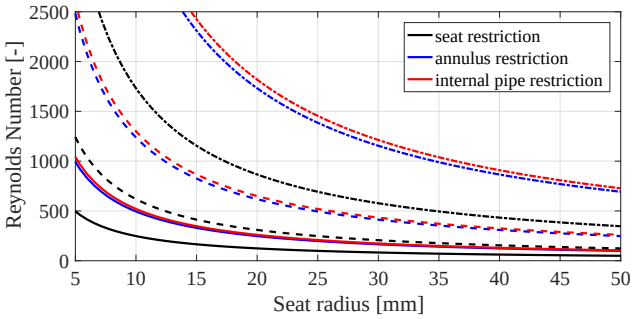

Figure 3: Analytical calculated Reynolds number at 100 (*full line*), 250 (*dashed lines*) and 700 (*dot-dashed lines*) L/min as a function of seat radius.

The critical Reynolds number Re_{c} i.e. where the flow transitions from laminar to turbulent is estimated using CFD analyses (described in details in Section 3). To this end, the relationship between the valve discharge coefficient and the Reynolds number is investigated for a wide range of flow magnitudes and valve seat diameters. Figure 4 shows the square-root of the Reynolds number versus the discharge coefficient C_{d}, calculated using $Q = A_{\text{d, seat}} C_{\text{d}} \sqrt{\frac{2}{\rho} \Delta p_{\text{valve}}}$, for two different stroke lengths and five different mean seat radii. The flow has been varied from -700 L/min to 700 L/min with a logarithmic distribution. Note that the negative Reynolds numbers shown in the figure indicate negative flow defined as flow exiting the fluid-domain through the bottom outlet bore holes and positive flows vice versa (see Figure 2). Common for all discharge coefficients are that the flow appears to be transitioning from laminar to turbulent at approximately $\text{Re} = 20^2 = 400$ since the discharge coefficient stabilizes (Merritt, 1967). Generally, smaller and more seat radius dependent discharge coefficients values are observed for negative flows, especially at the longer stroke length of 2.5 mm (upper figure). For designs having $L_{\text{stroke}} > \frac{W_{\text{seat}}}{2}$ the annulus flow area is smaller than the summed flow area of the seat restriction. In this case, the annulus restriction induces the majority of the valve pressure drop leading to significantly reduced flow forces on the moving member since the pressure drop across it is much smaller.

The discharge coefficient has also been calculated based on flow and pressure measurements performed on the active check-valve PT developed in Noergaard et al. (2016) (measurements are described in details in Section 6). Figure 5 shows the discharge coefficient and Reynolds number for different plunger positions. The flow appears to be transitioning at approximately $\text{Re} = 15^2 = 225$, which is slightly lower than for the

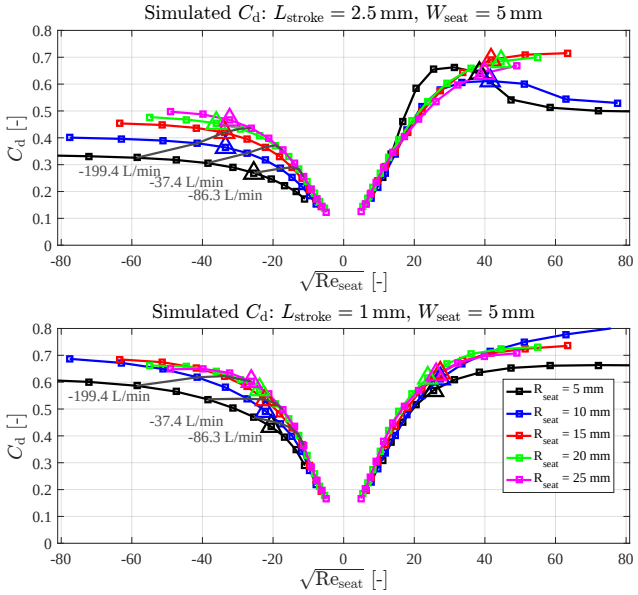

Figure 4: Calculated discharge coefficient as a function of the square-root of the Reynolds number for different seat diameters and stroke lengths. The grey lines indicate the corresponding flow rates and the triangles indicate a pressure drop of 1 bar.

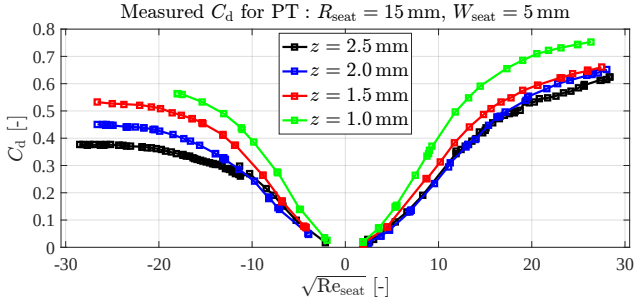

Figure 5: The discharge coefficient based on flow and pressure measurements on the active check-valve PT for different plunger positions.

simulation results in Figure 4. The 3D geometry in Figure 2 shows that the design is not axi-symmetric, as assumed in the simulations. This simplification is suspected to reduce the induced turbulence and thereby decrease the critical Reynolds number. The measurements show that a considerably higher discharge coefficient is achieved at smaller plunger positions, as the seat restriction is dominating the pressure drop. This corresponds well with the numerical results of Figure 4, which demonstrates larger discharge coefficients for the shorter stroke length of the lower plot, especially when conducting negative flow.

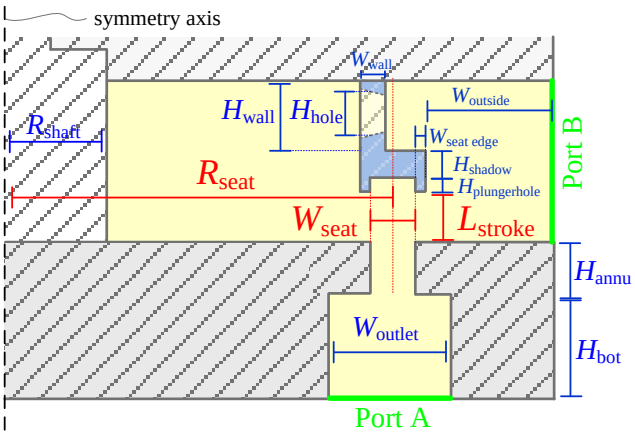

Figure 6: Geometric parametrization used when evaluating the CFD model. The red are design variables and the blue are design point auxiliary variables.

4 Parametrization of Geometry

The fluid domain is parametrized based on three design variables i.e. the stroke length L_{stroke}, the seat radius R_{seat} and the seat width W_{seat}. In addition to the design variables, the geometry is defined using a number of auxiliary variables that relates to the design variables. The seat and annular restriction of the valve are primarily rotation symmetric and are thus easy to convert into an axi-symmetric representation. The fluid inlet bore holes are not symmetric and therefore not possible to convert directly. Instead, an approximation is made based on the total flow area of the outlet holes by assuming another annular restriction with an appropriate flow area using a scaling coefficient $k_{port,A}$, based on the valve PT. Also, the radial holes of the valve plunger PT, allowing for flow across the inner valve seat edge, are not axi-symmetric and thus have been approximated using a similar approach. The geometry parametrization is shown in Figure 6 with additional information given in Table 1. From Table 1 it can be observed that several of the auxiliary variables defining the plunger geometry are set based on a scaling of the seat width. The force arising from pressure differences of several hundred bars when the valve is closed induces the structural dominant load, which scales proportionally with the seat width. The scaling of the auxiliary variables is set based on the PT valve. Also, to obtain a finer resolution at edges where the flow separates, all outward edges have been rounded with a fillet radius of 0.1 mm.

Table 1: Design variables with bounds and auxiliary variable definitions.

Design Vars.	**Bounds**	**PT value**
L_{stroke}	0.2/5 mm	2.5 mm
R_{seat}	7/50 mm	15 mm
W_{seat}	1/12 mm	5 mm
Depend. Vars.	**Definition**	**PT value**
R_{shaft}	$R_{\text{seat}}/5$	5.75 mm
W_{outlet}	$k_{\text{let}}(R_{\text{seat}}+W_{\text{seat}}/2)^2/2R_{\text{seat}}$	3.6 mm
W_{wall}	$2/5R_{\text{seat}}$	3.5 mm
H_{feet}	$W_{\text{seat}}/3$	1.7 mm
H_{shadow}	$W_{\text{seat}}/3$	1.3 mm
$W_{\text{seat edge}}$	$W_{\text{seat}}/5$	0.7 mm
H_{wall}	$R_{\text{seat}}2/5$	0.7 mm
H_{hole}	$H_{\text{wall}}/4$	1.6 mm
H_{bot}	$2\max(W_{\text{seat}}, L_{\text{stroke}})$	10 mm
H_{annu}	$\max(W_{\text{seat}}, L_{\text{stroke}})$	6 mm

5 Axi-Symmetric CFD

The numerical results presented throughout this paper are obtained using steady-state axi-symmetric CFD modeled in COMSOL 5.3. As shown in the previous section, the flow may be laminar or turbulent dependent on the valve geometry and flow rate. To accurately model the valve flow-field in both situations, both a laminar flow model and the RANS k-ϵ turbulence flow model are used when evaluating the design space. The deviations in simulated valve pressure drop and flow force are found to be small when comparing results obtained with the two models provided, if identical and sufficiently fine mesh is used. However, at larger Reynolds numbers, the Laminar model often fails to converge. In this case, the k-ϵ model was employed giving results for all query points. When evaluating the model throughout the design space, a rather larger number of model evaluations have been carried out. To reduce the computational effort, valve geometries which obviously lead to pressure drops much larger than allowed to enable efficient operation, are not evaluated. Using $\frac{Q^2}{A^2 C_{\text{d}}^2 \frac{2}{\rho}}$, with a conservative C_{d} value of 0.8, designs estimated to induce pressure drops above 5 bar are disregarded since high-efficient DDM operation not is considered feasible. The fluid domain is discretized primarily using triangular elements for the interior flow domain and quadrilateral elements to mesh boundary layers. To assess the necessary number of elements, the model is evaluated for different mesh densities using predefined mesh settings available in COMSOL, giving the x-axis of the results shown in Figure 7. Ten design points have been sampled randomly from the design space, for both the Laminar and the k-ϵ model, where the mesh has been gradually refined, using the predefined physics controlled mesh setting available in COMSOL. This means that different mesh

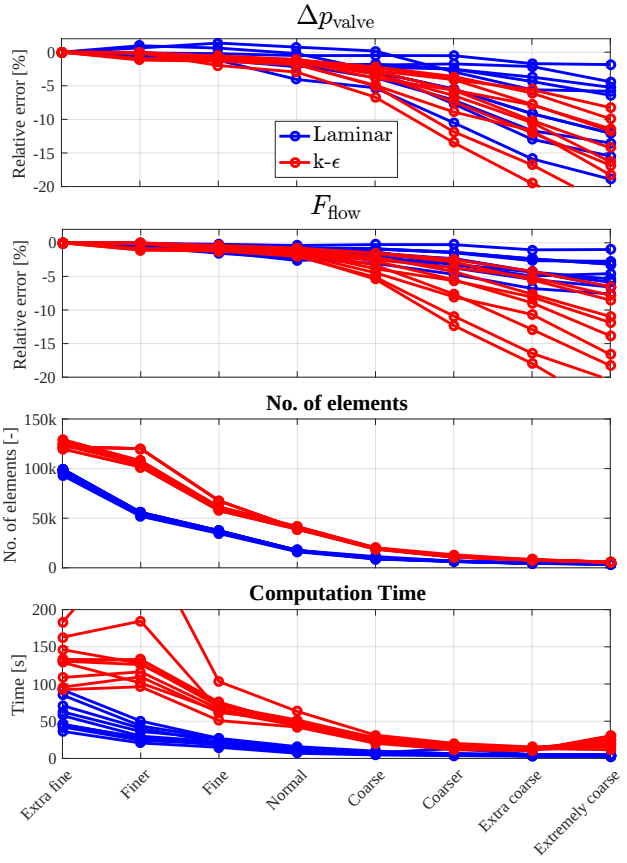

Figure 7: Relative errors, number of elements and computation time for 10 design points randomly sampled throughout the design space for both the Laminar and k-ϵ CFD model.

settings are used dependent on the model employed. The k-ϵ model requires a finer mesh. This is evident from the number of elements shown in Figure 7, which is larger when using the k-ϵ model. This, along with the k-ϵ model being more difficult to solve, leads to a computation time approximately three to five times larger than that of the Laminar model. The relative errors in Figure 7 are calculated relatively to the solution obtained using the 'Extra Fine' mesh resolution setting. The relative errors being primarily negative indicate that an absolute increase in both simulated pressure drop and flow force occur when refining the mesh. When using mesh resolutions finer than 'Normal', the deviations of both models are below 5%. To keep the computational burden at a manageable level the Laminar model is chosen with the mesh resolution 'Coarse' leading to an average model evaluation time 5 s.

Figure 8 and 9 show examples of the flow and pressure field throughout the fluid domain. Table 2 summarizes relevant information for both cases. The valve

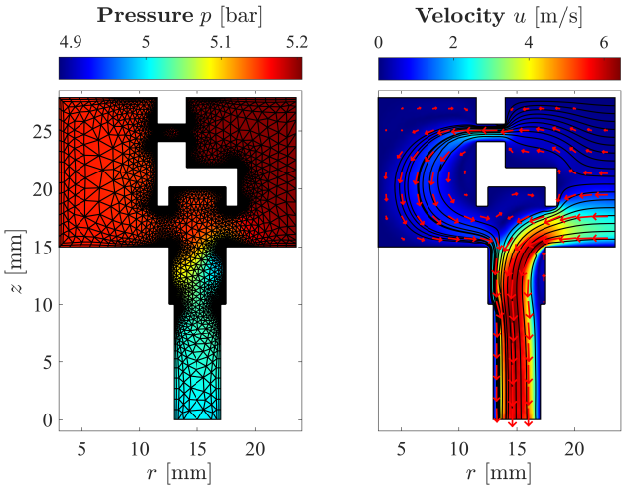

Figure 8: Pressure and velocity distributions for a flow rate of -120 L/min obtained using the Laminar model.

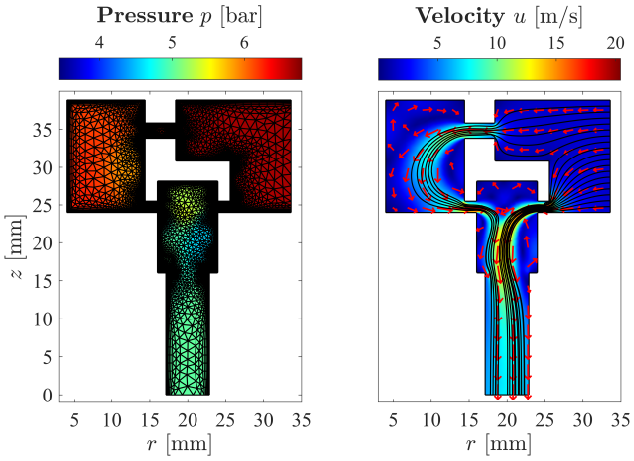

Figure 9: Pressure and velocity distributions for a flow rate of -300 L/min obtained using the k-ϵ model.

pressure drop is calculated as $\Delta p_{\text{valve}} = p_{\text{port B}} - p_{\text{port A}}$ where $p_{\text{port A}}$ and $p_{\text{port B}}$ are the average pressure at the fluid domain inlet and outlet. The axial flow force is calculated by integration of the pressure across the surfaces of the plunger geometry. The geometries are realized using the parametrization listed in Table 1 in Section 4. From the pressure distribution in Figure 8 it is seen that the largest pressure gradients occur at the annular restriction, opposed to Figure 9 where the largest pressure gradients occur at the seat restriction. This has significant influence on the magnitude of the axial flow forces.

Table 2: Information for the results in Fig. 8 and 9.

Design/Operation Point	**Fig. 8**	**Fig. 9**
$[L_{\text{stroke}}, R_{\text{seat}}, W_{\text{seat}}]$	[3.5, 15, 5]mm	[1.5, 20, 7]mm
Flow rate	-120 L/min	-300 L/min
Temperature	50 ° C	50 ° C
Outlet pressure	5 bar	5 bar
Working medium	VG-46 C	VG-46
Settings		
Mesh setting	Coarse	Coarse
# of elements	10762	20988
Simulation time	8 s	60 s
Flow model	Laminar	k-ϵ-RANS
Solver	PARDISO	MUMPS
Wall boundary conds.	no slip	wall funcs.
Inlet boundary conds.	mass flow rate	mass flow rate
Outlet boundary conds.	abs. pressure	abs. pressure
Results		
Pressure drop	-0.2 bar	-1.7 bar
Flow Force	-3.0 N	-191.9 N
C_{d}	0.57	0.85
Re_{seat}	198	371

6 Valve Prototype, Test Set-Up and Experimental Data

An active check-valve PT for DDMs has been designed and built (Noergaard et al., 2016) and is used to assess the accuracy of the developed CFD model. To facilitate testing the performance of PT valves in DDM operation, a commercial radial piston machine has been modified. One of the pressure chambers is retro-fitted with a custom-made valve block, connecting the pressure chamber to a high- and low-pressure manifold using two identical PT valves. When gathering the experimental data used to verify the CFD model, the port to the cylinder chamber has been blocked and both valves are kept open effectively short-circuiting the valve block. Using an external variable displacement pump station, steady flows are obtained while performing flow and pressure measurements. A differential pressure sensor was used with the measurements taken immediately up and downstream of the LPV valve, as shown in Figure 10 and in the CAD-model view of the valve block, with valves inserted, in Figure 11. The fluid domain of the PT valve design was shown in a sectional view in Figure 2 and Table 3 gives key specifications for the valve PT along with additional information about the test setup and measurement equipment.

Measurements of flow through and pressure difference across the low-pressure valve have been made for flows ranging from -140 to 140 L/min for different valve plunger positions and oil temperatures. The valve plunger position is kept fixed in an intermediate position by using spacers on the top side of the plunger. In addition to flow and pressure measure-

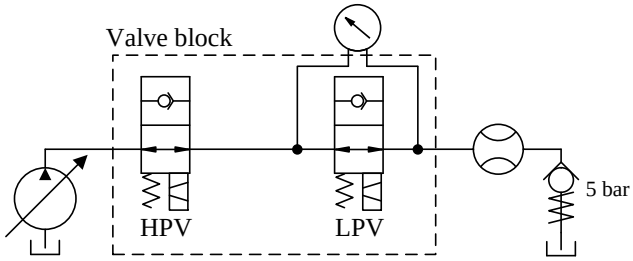

Figure 10: Hydraulic schematic of the setup used for experiments.

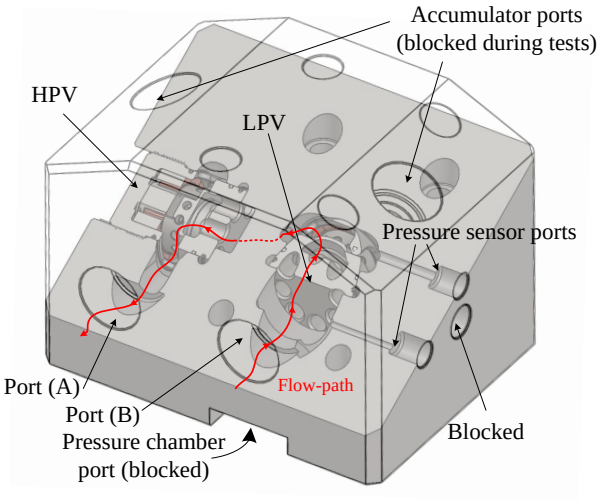

Figure 11: CAD-model showing the valve block used for experiments.

Table 3: Key specifications for the active check-valve PT and sensors used in experiments.

Valve specifications	
Actuation principle	Moving coil
Stroke length of actuator	2.5 mm
Valve dimensions	Ø 45 mm x 60 mm
Δp_{valve} @ nom. flow (±120 L/min)	+0.18/-0.48 bar
Valve closing time @ 48 V	3.2 ms
Mean electrical power @ 800 RPM	15-25 W
Opening spring force	30-35 N
Moving mass	33.4 g
Measurement equipment used in experiments	
Differential pressure sensor	HUBA control, type 692
Flow sensor	Parker, SCQ-150

ments, attempts to determine the magnitude of the flow force have been carried out. The valve is passively kept open by a spring installed to prevent closure of the valve, during negative flow, due to flow induced forces. In case the induced flow forces acting to close the valve exceed the pre-loading of the spring, the valve will close. By knowing the preloading of the spring, an

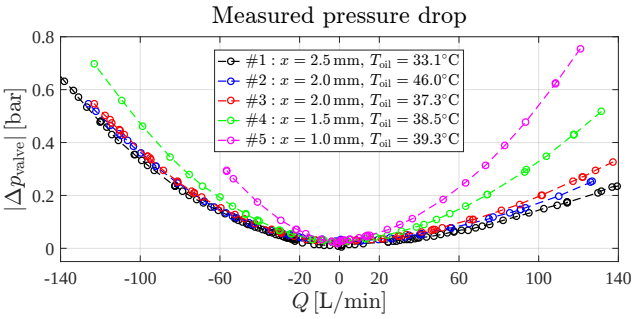

Figure 12: Measured pressure drop across the valve as a function of flow with different plunger positions and oil temperatures.

estimate of the flow force is obtained by increasing the flow rate slowly until the valve closes. Four different springs have been used enabling four flow force estimates at various plunger positions. Figure 12 shows the pressure drop measurements and Figure 13 shows the experimental flow force estimates besides simulated results to assess the accuracy of the model.

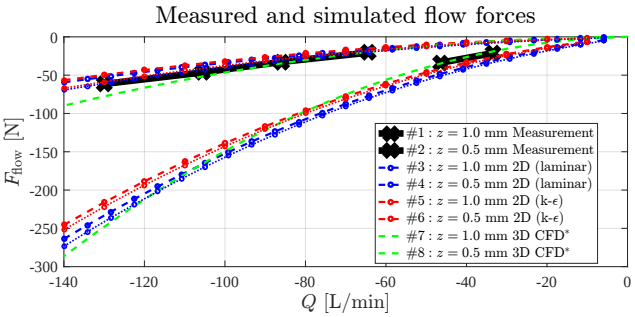

Figure 13: Estimated and simulated steady-state axial flow induced forces (sign convention in Fig. 3). Further information on the 3D CFD* simulation in Roemer et al. (2015). The dotted blue and red line represent the approximation based on the pressure difference i.e. $\Delta p_{\text{valve}} A_{\text{shadow}}$ using the Laminar and k-ϵ results respectively.

The flow versus pressure drop characteristics are seen to be flow direction dependent, with a pressure drop of 0.18 bar for negative flows and 0.48 bar for positive flows with a magnitude of 120 L/min, when the valve is fully opened. The pressure drop with the plunger fixed at 2 mm is shown at two different temperatures. From comparison of measurement 2 and 3, a slightly lower pressure drop is observed at elevated oil temperature since the oil viscosity is reduced. The pressure drop can be observed to only change slightly at larger plunger positions, whereas the pressure drop changes

significantly when the valve opening is smaller.

The flow versus fluid force measurements are shown in Figure 13 together with simulation results developed in Roemer et al. (2015) and when using the laminar and turbulent models (solver settings in Table 2). In total, six flow force estimates have been conducted experimentally. All the simulated flow forces show good coherence with measured data. The flow force estimate $2\pi R_{\text{seat}}(W_{\text{seat}} + 2W_{\text{seat,edge}})$ also shows good correlation. This has been observed to generally be a trend throughout the design space, but the correlation degrades for designs in which the seat edges do not induce the majority of the pressure loss across the valve (i.e. at relatively large stroke-lengths or small shadow areas).

To investigate the accuracy of the CFD model further, parts of the Q versus Δp_{valve} measurements are plotted together with simulated results. The results obtained using 3D CFD, shown in Figure 13 and 14, are described in detail in Roemer et al. (2015). Note that only data for negative flow was available from the 3D model. All models reveal correspondence with the measurements, however considerable deviation is observed for positive flows when the plunger position is $z = 2.5$ mm. The same mesh setting ('Coarse') has been utilized for both the Laminar and the k-ϵ model and the deviation in the results is seen to be small.

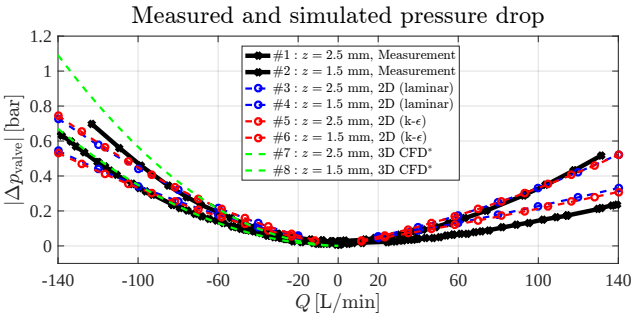

Figure 14: Simulated and measured valve pressure drops as a function of flow rate for different plunger positions.

7 Method for Loss Evaluation

To asses the suitability of a design point, both simulations of the valve pressure drop and flow force throughout the design space are used in combination with a simple model taken switching losses into account. The valve loss during one operation cycle is modeled as:

$$\begin{aligned} E_{\text{loss}} &= E_{\text{flow}} + \alpha E_{\text{switch}} \quad \text{where} \\ E_{\text{flow}} &= \int_0^{2\pi} Q(\theta)\Delta p_{\text{valve}}(Q(\theta))\mathrm{d}\theta \quad \text{and} \\ E_{\text{switch}} &= (E_{\text{passive}} + E_{\text{kin}}). \end{aligned} \tag{6}$$

The flow function is $Q(\theta) = Q_{\max}\sin(\theta)$ and the pressure drop Δp_{valve} is evaluated based on interpolation of the simulated CFD data. The displacement ratio α enables evaluating the losses at different displacement ratios[2]. The switching losses are split into kinetic losses E_{kin}, representing the losses related to acceleration of the moving member, and passive losses E_{passive}[3] representing the losses associated with closing the moving member against the passive opening element. For a full operating cycle, involving two active valve closings (one for each valve), the switching losses are modeled as:

$$\begin{aligned} E_{\text{passive}} &= 2L_{\text{stroke}}F_{\text{flow}}(Q_{\min})\frac{1}{\eta_{\text{act}}} \quad \text{and} \\ E_{\text{kin}} &= \left(\frac{L_{\text{stroke}}}{T_{\text{s}}(\dot{\theta})}\right)^2 \frac{M}{\eta_{\text{act}}}. \end{aligned} \tag{7}$$

The flow force is evaluated at the maximum negative flow rate given the maximum axial flow force acting to close the valve. The mass M is estimated as $(R_{\text{seat}} + W_{\text{seat}}/2)^2 k_{\text{mass}} + A_{\text{shadow}} k_{\text{virtual,mass}}$ where k_{mass} and $k_{\text{virtual,mass}}$ both are constants derived based on the PT design point and A_{shadow} is $2\pi W_{\text{seat}} R_{\text{seat}}$. The virtual mass represents surrounding oil that is accelerated during valve closing (virtual mass for PT is approximately 7.5 g, detailed information is given in Roemer et al. (2015)). The switching time $T_{\text{s}}(\dot{\theta})$ is set to be 5% of the revolution time ensuring the increase in flow loss due to valve switching is small (Roemer et al., 2013). The efficiency of the valve actuator is taken into account using η_{act}. The combined losses E_{loss} are normalized with the respect to the machine power using:

$$\epsilon_{\text{loss}} = \frac{E_{\text{loss}}}{\alpha E_{\text{in}}} = \frac{E_{\text{loss}}}{\alpha \Delta p_{\text{machine}} V_{\text{d}}} = \frac{E_{\text{loss}}\dot{\theta}}{\alpha \Delta p_{\text{machine}} Q_{\max}\pi}. \tag{8}$$

Using (8) optimal annular seat valve geometries are identified for different operating conditions and model parameters.

[2] Pumping and motoring operation cycles result in only positive or negative flow across the valves, respectively. This effect is not considered in this analysis. For evaluation of the flow losses, idling flows i.e. positive and negative flows are assumed.

[3] This is assuming the passive opening force is independent of the position. For springs, the force increases as the valve is closing, whereas using permanent magnets enables a latching mechanism that decreases when closing the valve.

8 Results

Figure 15 shows numerical results obtained using the CFD models described in Section 5. The upper plot shows the simulated valve pressure drop and the lower shows the simulated axial flow force, both for a flow rate of -278 L/min throughout the design space. The design space has been discretized design variable vectors:

$$L_{\text{stroke}} = [0.2,\ 0.4,\ 0.6,\ 1,\ 1.5,\ 2,\ 2.5,\ 3,\ 4,\ 5]\,\text{mm}$$
$$R_{\text{seat}} = [7,\ 10,\ 15,\ 25,\ 35,\ 50]\,\text{mm}$$
$$W_{\text{seat}} = [1,\ 1.5,\ 2,\ 3,\ 5,\ 8,\ 12]\,\text{mm}$$

This gives a total of $10 \times 6 \times 7 = 420$ different geometries. For each geometry design point the model is evaluated for 14 different flow rates. A logarithmic distribution is used for the flow:

$$Q_{\text{flow}} = \pm\,[6,\ 13,\ 28,\ 60,\ 129,\ 278,\ 600]\,\text{L/min}$$

This gives a total 5,880 model evaluations, but since some design combinations lead to infeasible geometries and other points have not been simulated since a pressure drop above 5 bar was estimated only 4,480 model evaluations are necessary. This was carried out in approximately 10 hours with an average model evaluation time 7 s, using a Intel Xeon E5-2665 2.4 GHz dual core CPU.

For better visualization the results have been interpolated to obtain a linear distribution in the geometry design space. Then, the method for evaluation of the valve losses, described in Section 7, is applied. Figure 16 shows the normalized loss ϵ_{loss} for three different combinations of maximum flow rate and valve switching time. For each of the three combinations, the coefficients k_{act} and k_{mass} have been varied to investigate the sensitivity. The displacement ratio is 100% in all cases and the machine pressure difference is 350 bar. To visualize which losses dominate inefficient designs, evaluation points having normalized losses above 2% are shown as either black, red or magenta. The color indicates which of the losses that are dominating: black is flow loss E_{flow}, red is the passive loss E_{passive} and magenta is the acceleration loss E_{kin}. Note, no evaluations are carried out for designs having large seat width and small seat radius since the geometries are infeasible. The results verify that high-efficient DDM operation is possible using annular seat valves. For all of the six different combinations of Figure 16, designs that enable operation with losses below 2% of the transferred power exist, even in case of an inefficient actuator and a relatively large moving mass.

The simulation case of $Q_{\text{max}} = 600$ L/min and $T_{\text{s}} = 3$ ms (1000 RPM), corresponds to the MHI DDM

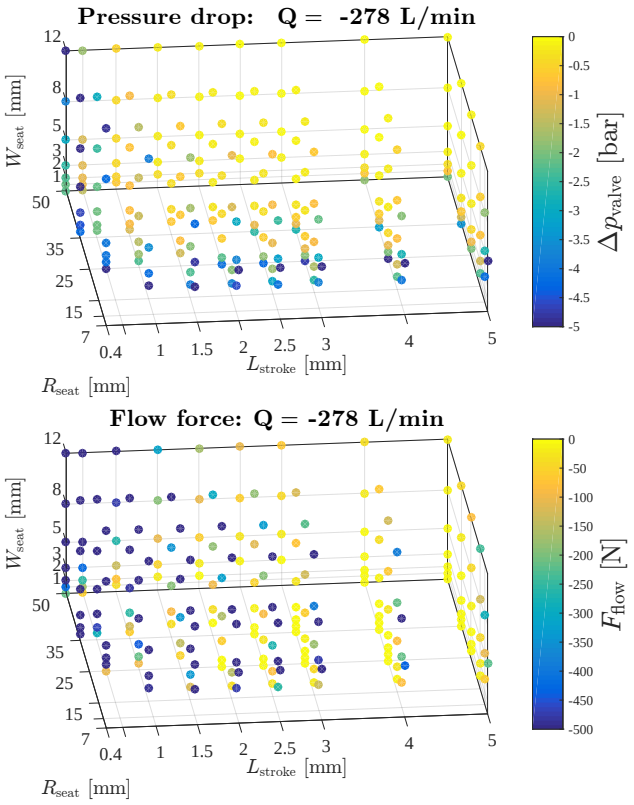

Figure 15: Numerical results throughout the design space for a flow rate of -278 L/min.

(Sasaki et al., 2014; Roemer et al., 2016). With valve coefficients corresponding to the PT (*left*), relatively large seat widths still enable efficient operation. With lower actuator efficiency, the seat width must be significantly smaller, since producing the required force leads to much greater losses.

The simulation case of $Q_{\text{max}} = 300$ L/min and $T_{\text{s}} = 1$ ms (3000 RPM), shows that efficient operation is possible using a wide range of valve geometries, even with a relatively large moving mass. The minimum valve losses are present for designs having a large stroke length and small seat radius.

The final simulation case of $Q_{\text{max}} = 100$ L/min and $T_{\text{s}} = 1$ ms (3000 RPM), shows that efficient operation is possible using a wide range of valve geometries with valve parameters similar to the PT. However, if both having an efficient actuator and a relatively heavy moving mass, the switching related losses increase significantly. In this case, efficient DDM operation is still possible but the design space is much narrower.

9 Conclusion & Outlook

Using axi-symmetric CFD analysis for numerous different annular seat valve designs, it was verified that high-efficient DDM operation is possible, even with relatively inefficient actuators and relatively heavy valve plungers. In case of efficient actuators and a low moving mass, the valve plunger geometry may be chosen relatively freely. The feasible design space enabling high-efficient DDM shrinks if the valve actuator is inefficient. The valve design points yielding the highest efficiencies were shown to have large stroke lengths, large seat radii, but small seat width. This is because the flow forces reduce significantly for stroke lengths larger than half of the seat width. For large stroke lengths the seat flow area is larger than the annulus area, hence the annulus induces the dominating pressure loss. This effect may be utilized in the active check-valves of DDMs, and possible other applications, to reduce the force requirements of the actuator (A valve utilizing a similar principle, including feedback of an intermediate pressure state, is demonstrated in Lauttamus et al. (2007)).

Besides the switching and flow losses of the valves, friction and leakage losses between lubricating surfaces may influence the machine efficiency drastically (Sorensen et al., 2012). However, in the case of DDMs using seat valves, the leakage losses are reduced significantly, since losses at the port-plate typically used for commutation are avoided.

The difference in flow forces and pressure drops, when using either a Laminar model or a RANS k-ϵ turbulence, was shown to be small when using sufficiently fine mesh. Pressure drops and flow forces were measured, using an active check-valve prototype, which demonstrated that the simplified 2D axi-symmetric representation of the actual 3D geometry deviate less than approximately 5%.

The pressure drop characteristics were shown to be flow-direction dependent through simulations and measurements. The flow forces and valve pressure drops are largest for negative flows (defined in Figure 2) which results in a slightly lower efficiency for motoring cycles than for pumping cycles. For high-efficient operation (low valve pressure drop relative to the machine pressure difference), this effect does not influence the losses significantly, but at less efficient operation it is more pronounced.

Acknowledgments

The research presented in this paper has received funding from the Norwegian Research Council through the SFI Offshore Mechatronics project (project number 237896) and the Danish Strategic Research Council through the HyDrive Project (project number 130500038B).

References

Heikkila, M. *Energy Efficient Boom Actuation Using a Digital Hydraulic Power Management System*. Ph.D. thesis, Tampere University of Technology, 2016.

Heikkila, M., Tammisto, J., Huova, M., Huhtala, K., and Linjama, M. Experimental evaluation of a piston-type digital pump-motor-transformer with two independent outlets. In *Proc. of ASME/Bath Fluid Power and Motion Control*. Bath, UK, pages 83–97, 2010.

Holland, M. A., Merrill, K. J., and Lumkes, J. H. Experimental evaluation of digital pump/motor operating strategies with a single-piston pump/motor. In *Proc. of the 52nd National Conference on Fluid Power*. Las Vegas, US, 2011.

Lauttamus, T., Linjama, M., Nurmia, M., and Vilenius, M. A novel seat valve with reduced axial forces. In *Proc. of Power Transmission And Motion Control*. Bath, UK, pages 415–427, 2007.

Linjama, M. and Huhtala, K. Digital pump-motor with independent outlets. In *Proc. of the 11th Scandinavian International Conference on Fluid Power*. Linköbing , Sweden, 2009.

Merrill, K. J., Holland, M. A., and Lumkes, J. H. Efficiency analysis of a digital pump/motor as compared to a valve plate design. In *Proc. of the 7th International Fluid Power Conference*. Aachen, Germany, 2010.

Merritt, H. E. *Hydraulic control systems*. New York, Wiley, 1967.

Noergaard, C., Bech, M. M., Roemer, D. B., and Pedersen, H. C. Optimisation of moving coil actuators for digital hydraulic machines. In *Proc. of the 8$^{\text{th}}$ Workshop on Digital Fluid Power*. Tampere, Finland, pages 39–54, 2016.

Nordaas, S., Andersen, T. O., and Ebbesen, M. K. Feasibility study of a digital hydraulic winch system. In *Proc. of the Ninth Workshop on Digital Fluid Power*. Aalborg, Denmark, 2017.

Rampen, W. The development of digital displacement technology. In *Proc. of the Fluid Power & Motion Control*. ASME/Bath, Bath, UK, pages 12–17, 2010. Keynote adress.

Roemer, D. B. *Design and Optimization of Fast Switching Valves for Large Scale Digital Hydraulic Motors*. Ph.D. thesis, Department of Energy Technology, Aalborg University, 2014.

Roemer, D. B., Johansen, P., Pedersen, H., and Andersen, T. Analysis of valve requirements for high-efficiency digital displacement fluid power motors. In *Proc. of the 8th International Conference on Fluid Power Transmission and Control*. Hangzhou, China, pages 122–126, 2013.

Roemer, D. B., Johansen, P., Schmidt, L., and Andersen, T. O. Modeling of movement-induced and flow-induced fluid forces in fast switching valves. In *Proc. of 2015 International Conference on Fluid Power and Mechatronics*. Harbin, China, pages 978–983, 2015. doi:10.1109/FPM.2015.7337257.

Roemer, D. B., Noergaard, C., Bech, M. M., and Johansen, P. Valve and manifold considerations for digital hydraulic machines. In *Proc. of the 8th Workshop on Digital Fluid Power*. Tampere, Finland, pages 213–227, 2016.

Sasaki, M., Yuge, A., Hayashi, T., Nishino, H., Uchida, M., and Noguchi, T. Large capacity hydrostatic transmission with variable displacement. In *Proc. of the 9th International Fluid Power Conference*. Aachen, Germany, 2014.

Soerensen, R. M., Hansen, M. R., and Mouritsen, O. Numerical and Experimental Study of Friction Loss in Hydrostatic Motor. *Modeling, Identification and Control*, 2012. 33(3):99–109. doi:10.4173/mic.2012.3.2.

Tammisto, J., Huova, M., Heikkil, M., Linjama, M., and Huhtala, K. Measured characteristics of an in-line pump with independently controlled pistons. In *Proc. of the 7th International Fluid Power Conference*. Aachen, Germany, pages 1–12, 2010.

Taylor, J., Rampen, W., Abrahams, D., and Latham, A. Demonstration of a digital displacement hydraulic hybrid - a globally affordable way of saving fuel. In *Proc. of the Annual JSAE Congress*. Pacifico Yokohama, Japan, 2015.

Taylor, J., Rampen, W., Robertson, A., and Caldwell, N. Digital displacement hydraulic hybrids - parallel hybrid drives for commercial vehicles. Technical report, Artemis Intelligent Power, Ltd., Paper presented at the annual JSAE congress, Kyoto, Japan, 2011.

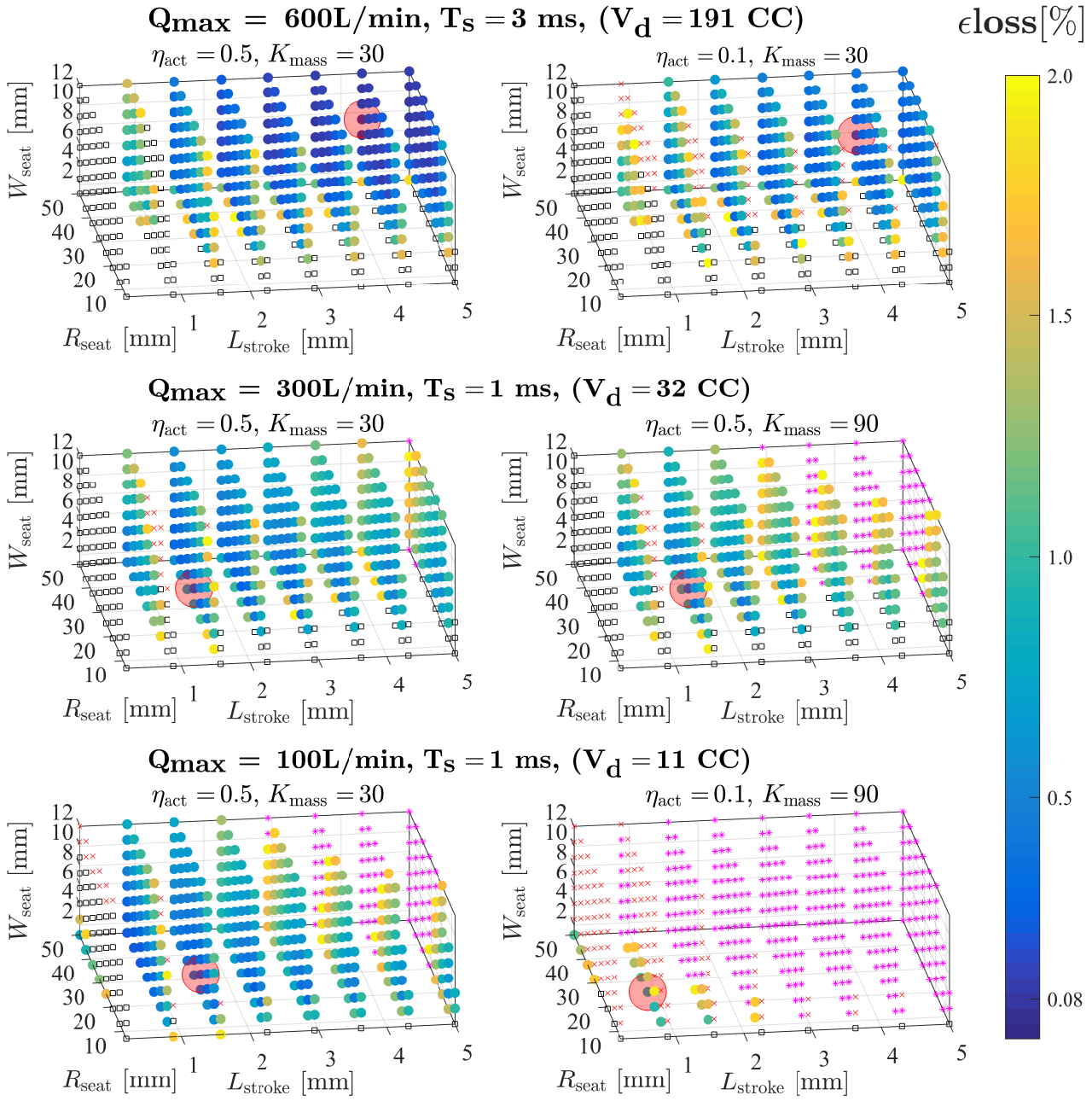

Figure 16: Relative valve losses throughout the design space, for different flow rates and valve switching times and model coefficients. The black, red and magenta points represent designs where $\epsilon_{loss} > 2\%$ and the colors indicate which loss is dominant: black square is flow loss, red cross is the passive loss, and magenta star is the acceleration loss. The larger opaque red circles indicate the optimum valve sizing for the respective operating conditions.